Drug-Loaded and Superparamagnetic Iron Oxide Nanoparticle Surface-Embedded Amphiphilic Block Copolymer Micelles for Integrated Chemotherapeutic Drug Delivery and MR Imaging

Jinming Hu,[†] Yinfeng Qian,[*,‡] Xiaofeng Wang,[†] Tao Liu,[†] and Shiyong Liu[*,†]

[†]CAS Key Laboratory of Soft Matter Chemistry, Hefei National Laboratory for Physical Sciences at the Microscale, Department of Polymer Science and Engineering, University of Science and Technology of China, Hefei, Anhui 230026, China

[‡]The First Affiliated Hospital of Anhui Medical University, Hefei, Anhui 230022, China

S *Supporting Information*

ABSTRACT: We report on the fabrication of organic/inorganic hybrid micelles of amphiphilic block copolymers physically encapsulated with hydrophobic drugs within micellar cores and stably embedded with superparamagnetic iron oxide (SPIO) nanoparticles within hydrophilic coronas, which possess integrated functions of chemotherapeutic drug delivery and magnetic resonance (MR) imaging contrast enhancement. Poly(ε-caprolactone)-*b*-poly(glycerol monomethacrylate), PCL-*b*-PGMA, and PCL-*b*-P(OEGMA-*co*-FA) amphiphilic block copolymers were synthesized at first by combining ring-opening polymerization (ROP), atom transfer radical polymerization (ATRP), and post- modification techniques, where OEGMA and FA are oligo(ethylene glycol) monomethyl ether methacrylate and folic acid-bearing moieties, respectively. A model hydrophobic anticancer drug, paclitaxel (PTX), and 4 nm SPIO nanoparticles were then loaded into micellar cores and hydrophilic coronas, respectively, of mixed micelles fabricated from PCL-*b*-PGMA and PCL-*b*-P(OEGMA-*co*-FA) diblock copolymers by taking advantage of the hydrophobicity of micellar cores and strong affinity between 1,2-diol moieties in PGMA and Fe atoms at the surface of SPIO nanoparticles. The controlled and sustained release of PTX from hybrid micelles was achieved, exhibiting a cumulative release of ~61% encapsulated drugs (loading content, 8.5 w/w%) over ~130 h. Compared to that of surfactant-stabilized single SPIO nanoparticles (r_2 = 28.3 s^{-1} mM^{-1} Fe), the clustering of SPIO nanoparticles within micellar coronas led to considerably enhanced T_2 relaxivity (r_2 = 121.1 s^{-1} mM^{-1} Fe), suggesting that hybrid micelles can serve as a T_2-weighted MR imaging contrast enhancer with improved performance. Moreover, preliminary experiments of in vivo MR imaging were also conducted. These results indicate that amphiphilic block copolymer micelles surface embedded with SPIO nanoparticles at the hydrophilic corona can act as a new generation of nanoplatform integrating targeted drug delivery, controlled release, and disease diagnostic functions.
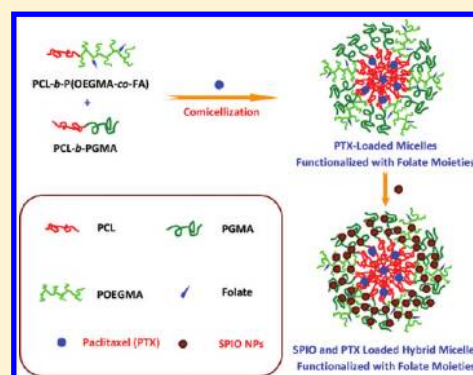
■ INTRODUCTION

Cancer chemotherapy and diagnostic imaging using metallic or inorganic nanoparticles have attracted ever-increasing attention in the past decades due to their unique physical characteristics and the capability of targeting specific disease areas.[1−6] Among them, monodisperse magnetic nanoparticles, such as superparamagnetic iron oxide (SPIO) nanoparticles, possess combined advantages such as guided in vivo transport under external magnetic field, T_2-type magnetic resonance (MR) imaging contrast enhancement, and hyperthermia cancer therapy under alternating magnetic field.[7−12] Thus, magnetic nanoparticles have found practical applications in diverse fields such as MR diagnostic imaging, biosensing systems with enrichment, capturing, and amplifying functions, and targeted delivery nanovehicles for therapeutic agents (e.g., chemotherapeutic drugs, DNA, and small interfering RNA (siRNA)).[13−18] Currently, a huge research impetus has been input to develop hybrid SPIO nanoparticles integrated with multiple imaging, detection, and drug delivery functions.[1−3,19,20]

To further enhance the functions of metallic or inorganic nanoparticles, a variety of strategies have been developed to fabricate stable clusters or controlled assemblies of single nanoparticles.[19−21] For example, clusters of gold or silver nanoparticles can be employed for Raman signal amplifying due to the creation of Raman hotspots from closely packed nanoparticles and local electromagnetic coupling effect.[22−24] Concerning magnetic nanoparticles, although well-dispersed SPIO nanoparticles have been clinically applied for MR imaging contrast enhancement, they typically possess relatively low magnetization and are difficult to be guided and manipulated with an external magnetic field; whereas clusters of SPIO nanoparticles have shown much better MR imaging contrast

enhancement and considerably larger responses under external magnetic field.[25−29]

Amphiphilic and double hydrophilic block copolymers can direct the controlled clustering or assembly of SPIO nanoparticles either via hydrophobic encapsulation within micellar cores or electrostatic interactions between surface charged hydrophilic SPIO nanoparticles and block polyelectrolytes, and considerable MR imaging contrast enhancement was achieved as a result of the collective effects of SPIO nanoparticle clusters or assemblies.[25−30] To achieve good colloidal stability applicable under physiological media, these SPIO nanoparticle clusters are typically stabilized by hydrophilic coronas of poly(ethylene oxide) (PEO), poly(oligo(ethylene glycol) monomethyl ether methacrylate) (POEGMA), polyacrylamide, or zwitterionic polymer segments. Additionally, it has been well-established that micelles and vesicles assembled from block copolymers can act as controlled-release nanocarriers of hydrophobic chemotherapeutic drugs.[31−35] Thus, block copolymer micelles embedded with multiple SPIO nanoparticles and anticancer drugs are capable of integrated drug delivery and enhanced MR imaging functions, which are quite beneficial for combined cancer diagnostics and chemotherapy and the facile monitoring of chemotherapeutic efficacy.[1−3]

On the other hand, almost all previous examples concerning block copolymer-directed iron oxide nanoparticle clusters involve the fabrication of hybrid micelles with inorganic nanoparticles embedded within the micellar cores. For example, Gao et al.[27] reported the preparation of amphiphilic block copolymer micelles with the hydrophobic cores loaded with T_2-type SPIO nanoparticles, and ∼7 times enhancement in T_2 relaxivity (r_2) was achieved compared to single SPIO nanoparticles. The micellar cores can also be coloaded with SPIO nanoparticles and hydrophobic chemotherapeutic drug (doxorubicin, DOX) to enable dual functions of drug delivery and MR imaging.[36,37] Hydrophilic SPIO nanoparticles can also be loaded into the aqueous hollow interior of cross-linked vesicles fabricated from amphiphilic ABA triblock copolymers, and chemotherapeutic drugs were physically or covalently attached to the hydrophobic vesicle bilayers.[38,39] By utilizing electrostatic interactions, micellar nanoparticles embedded with iron oxide nanoparticle clusters can also be fabricated from cationic-neutral block polyelectrolytes and negatively charged iron oxide nanoparticles, as originally reported by the Berret[29] and Held[30] research groups.

Although the clustering of SPIO nanoparticles within polymeric micellar cores can lead to T_2-type MR imaging contrast enhancement, currently, there lacks quantitative understanding of the underlying mechanism. It was implied that the interaction of water molecules with SPIO nanoparticle-loaded hybrid micelles contributes to the contrast enhancement, as compared to that of single SPIO nanoparticles. We are quite curious about when hydrophilic SPIO nanoparticles are embedded into the well-solvated corona of amphiphilic block copolymer micelles, can we still achieve the T_2-type MR imaging contrast enhancement? In this case, hydrophobic drugs and hydrophilic SPIO nanoparticles can be respectively loaded into micellar cores and coronas, which should be quite beneficial for the elevation of drug loading content and the elimination of undesirable interactions between chemotherapeutic drugs and SPIO nanoparticles. It is expected that this new type of design will further enrich the theranostic nanoplatform design as compared to previous reports concerning the coencapsulation of drugs and SPIO nanoparticles solely into the hydrophobic micellar cores.[27,28]

Scheme 1. Schematic Illustration of the Fabrication of Hybrid Micelles Comprising Hydrophobic PCL Cores and Mixed PGMA/P(OEGMA-*co*-FA) Hydrophilic Coronas Embedded with 4 nm SPIO Nanoparticles from PCL-*b*-PGMA and PCL-*b*-P(OEGMA-*co*-FA) Diblock Copolymers
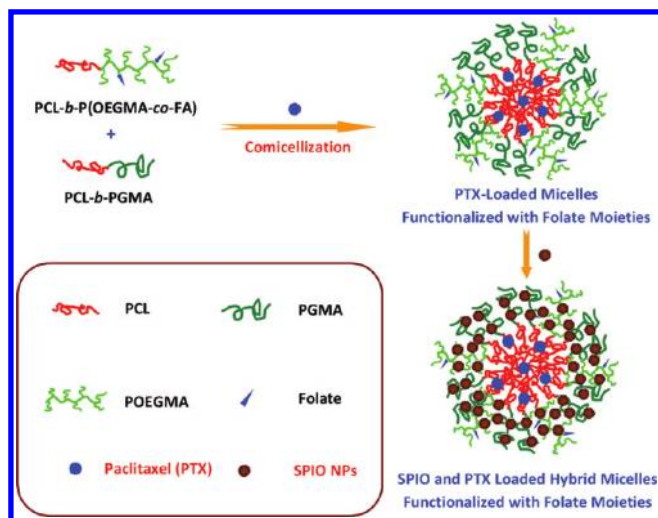

Herein, we report on the fabrication of organic/inorganic hybrid micelles of amphiphilic diblock copolymers with the micellar cores physically encapsulated with hydrophobic drugs and hydrophilic coronas stably embedded with SPIO nanoparticles, which possess integrated functions of chemotherapeutic drug delivery and MR imaging contrast enhancement (Scheme 1). To achieve this, poly(ε-caprolactone)-*b*-poly-(glycerol monomethacrylate), PCL-*b*-PGMA, and PCL-*b*-P-(OEGMA-*co*-FA) amphiphilic diblock copolymers were synthesized at first via a combination of ring-opening polymerization (ROP), atom transfer radical polymerization (ATRP), and postfunctionalization techniques, where OEGMA and FA are oligo(ethylene glycol) monomethyl ether methacrylate and folic acid-bearing moieties, respectively (Scheme 2). A model hydrophobic drug, paclitaxel (PTX), and 4 nm SPIO nanoparticles were then loaded into micellar cores and hydrophilic coronas, respectively, of mixed micelles fabricated from PCL-*b*-PGMA and PCL-*b*- P(OEGMA-*co*-FA) diblock copolymers by taking advantage of the hydrophobicity of micellar cores and the strong affinity between 1,2-diol moieties in PGMA and Fe atoms at the surface of SPIO nanoparticles.[40] Subsequently, the controlled release characteristics, and in vitro and in vivo MR imaging contrast enhancement performance of drug-loaded and SPIO nanoparticle surface embedded polymeric micelles were examined. It was found that amphiphilic diblock copolymer micelles surface embedded with SPIO nanoparticles at hydrophilic coronas can serve as a new generation of nanoplatforms integrating targeted drug delivery, controlled release, and disease diagnostic functions.

■ EXPERIMENTAL PART

Materials. ε-Caprolactone (ε-CL, Fluka, ≥99%) was dried over CaH_2 and distilled under reduced pressure. OEGMA (M_n = 475 g/mol, mean degree of polymerization, DP, is 8−9) purchased from Aldrich was passed through a neutral alumina column to remove the inhibitor and then stored at −20 °C prior to use. N,N,N',N'',N''-Pentamethyldiethylenetriamine

Scheme 2. Synthetic Routes Employed for the Preparation of PCL$_{70}$-*b*-PGMA$_{40}$ and PCL$_{70}$-*b*-P(OEGMA$_{0.95}$-*co*-FA$_{0.05}$)$_{60}$ Diblock Copolymers
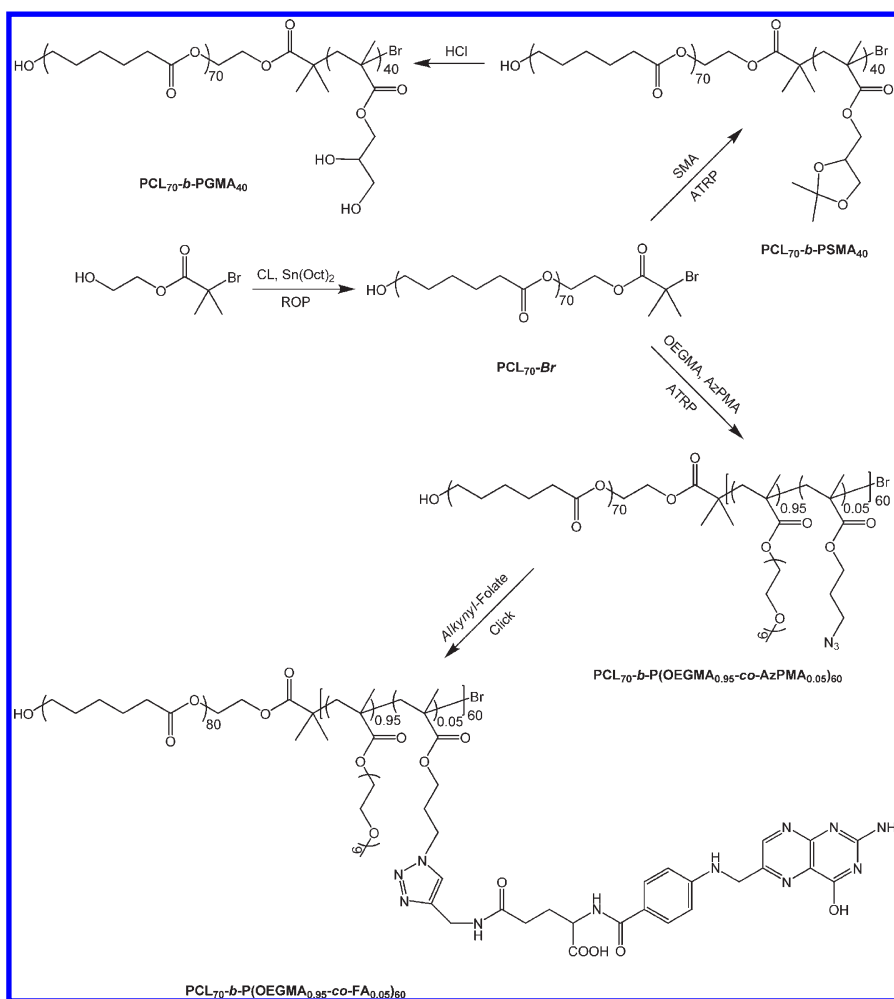


(PMDETA, 98%), copper(I) bromide (CuBr, 98%), stannous(II) octanoate (Sn(Oct)$_2$, 95%), and PTX were purchased from Aldrich and used as received. Sodium azide (NaN$_3$, 99%, Alfa Aesar), propargylamine (99%, Aldrich), solketal (97%, Aldrich), and cetyltrimethylammonium bromide (CTAB) were used as received. 3-Azidopropyl methacrylate (AzPMA),[41] alkynyl-functionalized folic acid (*alkynyl*-FA),[42] solketal methacrylate (SMA),[43,44] 2-hydroxyethyl 2-bromo-2-methylpropanoate (HBMP),[45] and CTAB-stabilized 4 nm SPIO nanoparticles[46] were synthesized according to literature procedures.

Sample Synthesis. *Synthesis of PCL-Br ATRP Macroinitiator (Scheme 2).* PCL-Br macroinitiator was synthesized via the ROP of ε-CL in anhydrous toluene using HBMP as the initiator and Sn(Oct)$_2$ as the catalyst (Scheme 2). In a typical example, HBMP (0.23 g, 1.09 mmol), ε-CL (10.0 g, 87.6 mmol), and 20 mL of dry toluene were added into a Schlenk flask equipped with a magnetic stirring bar. About 5 mL of toluene was removed under reduced pressure at first. Then, 0.15 mL of Sn(Oct)$_2$ solution in dry toluene (1.0 g/mL) was added under nitrogen protection. After removing another 5 mL of toluene under reduced pressure, the flask was carefully sealed under vacuum and stirred at 62 °C for 12 h. The flask was then quenched into liquid nitrogen to terminate the polymerization. The reaction mixture was diluted with tetrahydrofuran (THF) and then precipitated into an excess of methanol. The purification cycle of dissolution in THF and precipitation into methanol was then repeated twice. Finally, the precipitates were collected by filtration and dried in a vacuum oven at room temperature

for 24 h (8.2 g, yield: 80%). The molecular weight and molecular weight distribution of the product were determined by gel permeation chromatography (GPC) using dimethylformamide (DMF) as the eluent, revealing an M_n of 9.6 kDa and an M_w/M_n of 1.05. The DP of PCL-Br was determined to be 70 by ^{1}H NMR analysis in CDCl$_3$ (Figure 1a); thus, the PCL-based ATRP macroinitiator was denoted as PCL$_{70}$-Br.

Synthesis of PCL-b-P(OEGMA-co-AzPMA) Block Copolymer (Scheme 2). PCL-*b*-P(OEGMA-*co*-AzPMA) block copolymer was synthesized via the ATRP of OEGMA and AzPMA comonomers in anisole at 30 °C using PCL$_{70}$-Br as the macroinitiator. In a typical example, PCL$_{70}$-Br (0.5 g, 0.06 mmol bromine initiating moieties), OEGMA (2.85 g, 6 mmol), AzPMA (0.05 g, 0.3 mmol), PMDETA (10 mg, 0.06 mmol), and anisole (5 mL) were added into a Schlenk flask equipped with a magnetic stirring bar. The mixture was carefully degassed by three freeze−pump−thaw cycles, and CuBr (9 mg, 0.06 mmol) was introduced under the protection of nitrogen flow. The flask was then sealed under vacuum and placed in an oil bath thermostatted at 30 °C. After 4 h, the flask was quenched into liquid nitrogen to terminate the polymerization. The reaction mixture was diluted with THF and passed though a silica gel column to remove copper catalyst. After removing most of the solvent, the product was purified by repeated precipitation into petroleum ether to remove unreacted monomer, and then dried in a vacuum oven overnight at room temperature, affording ∼1.75 g of a white sticky solid (yield: 51.5%). GPC analysis revealed an M_n of 24.7 kDa and an M_w/M_n of 1.12. The monomer conversions of OEGMA and AzPMA were determined to be 49.8% and 51.2%, respectively, on the basis of
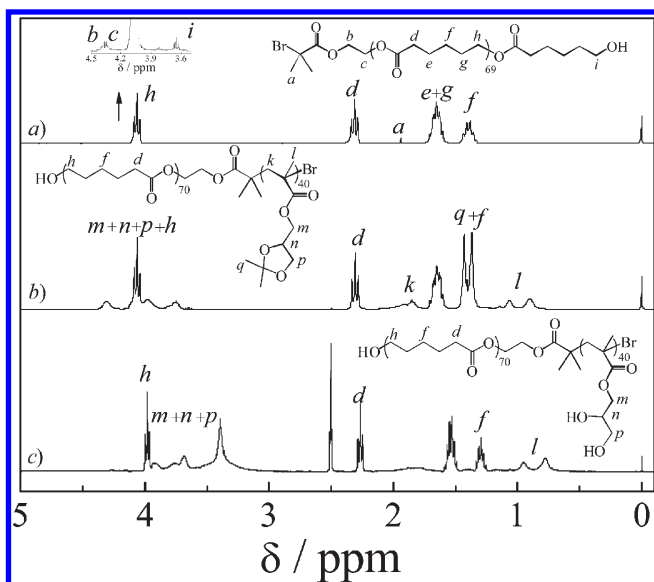
Figure 1. ^{1}H NMR spectra recorded for (a) PCL$_{70}$-Br ATRP macro-initiator in CDCl$_3$, (b) PCL$_{70}$-b-PSMA$_{40}$ in CDCl$_3$, and (c) PCL$_{70}$-b-PGMA$_{40}$ in DMSO-d_6.

^{1}H NMR analysis of the polymerization mixture just before purification. Due to the overlapping of NMR resonance signals characteristic of OEGMA and AzPMA moieties within the P(OEGMA- co-AzPMA) block, the OEGMA/AzPMA molar ratio in the copolymer block was estimated from monomer conversions. In combination with the M_n data determined from GPC, the chemical structure of the product was determined to be PCL$_{70}$-b-P(OEGMA$_{0.95}$-co- AzPMA$_{0.05}$)$_{60}$.

Synthesis of PCL$_{70}$-b-P(OEGMA$_{0.95}$-co-FA$_{0.05}$)$_{60}$ Amphiphilic Diblock Copolymer (Scheme 2). The target product, PCL$_{70}$-b-P(OEGMA$_{0.95}$-co-FA$_{0.05}$)$_{60}$, was synthesized via the click reaction of PCL$_{70}$-b-P-(OEGMA$_{0.95}$-co-AzPMA$_{0.05}$)$_{60}$ with *alkynyl*-FA. Typically, *alkynyl*-FA (124 mg, 0.26 mmol), PMDETA (19 mg, 0.11 mmol), PCL$_{70}$-b-P(OEGMA$_{0.95}$-co-AzPMA$_{0.05}$)$_{60}$ (1.0 g, 0.08 mmol azide moieties), and dimethyl sulfoxide (DMSO; 6 mL) were added into a reaction flask. The flask was carefully degassed via three freeze−pump−thaw cycles, and CuBr (16 mg, 0.11 mmol) was then introduced under the protection of nitrogen flow. Subsequently, the flask was sealed under vacuum and placed in an oil bath thermostatted at 40 °C. After 24 h, the flask was quenched into liquid nitrogen. The reaction mixture was diluted with THF and passed though a silica gel column to remove copper catalyst. After removing most of the solvent, the residues were subjected to dialysis against deionized water (MW cutoff ∼7.0 kDa) for 36 h. The final product, PCL$_{70}$-b-P(OEGMA$_{0.95}$-co- FA$_{0.05}$)$_{60}$, was obtained via lyophilization.

Synthesis of PCL-b-PGMA Diblock Copolymer (Scheme 2). PCL$_{70}$-b-PSMA$_{40}$ diblock copolymer was synthesized at first via the ATRP of SMA monomer in cyclohexanone at 80 °C using PCL$_{70}$-Br as the ATRP macroinitiator. In a typical procedure, PCL$_{70}$-Br (0.5 g, 0.06 mmol bromine initiating moieties), SMA (0.5 g, 2.5 mmol), PMDETA (10 mg, 0.06 mmol), and cyclohexanone (5.0 mL) were charged into a Schlenk flask equipped with a magnetic stirring bar. The flask was then carefully degassed via three freeze−pump−thaw cycles, and then CuBr (9 mg, 0.06 mmol) was introduced under the protection of nitrogen flow. The flask was sealed under vacuum and placed in an oil bath thermostatted at 80 °C. After 5 h, the flask was quenched into liquid nitrogen to terminate the polymerization. The reaction mixture was diluted with THF and passed though a neutral alumina column to remove copper catalysts. After removing most of the solvent, the product was precipitated into petroleum ether. The sediments were collected via filtration and then

dried in a vacuum oven overnight at room temperature, affording ∼0.9 g of white solid (yield: 90%). GPC analysis revealed an $M_{n,GPC}$ of 12.6 kDa and an M_w/M_n of 1.12. ^{1}H NMR analysis revealed a DP of 40 for the PSMA block (Figure 1b). Thus, the diblock copolymer was denoted as PCL$_{70}$-b-PSMA$_{40}$.

For the synthesis of PCL$_{70}$-b-PGMA$_{40}$ diblock copolymer, PCL$_{70}$-b-PSMA$_{40}$ (0.60 g) was dissolved in 50 mL of 1,4-dioxane. After cooling to 0 °C in an ice/water bath, 6.0 mL aqueous HCl (1.0 N) was added dropwise. After the addition process was finished, the reaction mixture was further stirred at room temperature for 3 h. The mixture was then precipitated into petroleum ether. This dissolution−precipitation cycle was repeated twice. The final product was collected by filtration and then dried in a vacuum oven overnight at room temperature (0.5 g, yield: 92.5%).

Preparation of Organic/Inorganic Hybrid Mixed Micelles. In a typical example, 20 mg of PCL$_{70}$-b-PGMA$_{40}$ and 4 mg of PCL$_{70}$-b-P(OEGMA$_{0.95}$-co-FA$_{0.05}$)$_{60}$ were first dissolved in 1.0 mL ethanol at 60 °C. Subsequently, 9 mL of deionized water (50 °C) was quickly injected under vigorous stirring. The formation of micelles quickly occurred, as indicated by the appearance of the bluish tinge characteristic of colloidal dispersions. After cooling to room temperature, a varying amount of aqueous dispersion of CTAB-stabilized SPIO nanoparticles (1.0 g/L) was added to achieve different target SPIO nanoparticle loading contents ($W_{SPIO}/W_{micelles}$: 0, 1.25, 2.5, 5, 10 w/w%). After magnetic stirring for 12 h, the dispersion was transferred into a dialysis tubing (MW cutoff ∼3.0 kDa) and dialyzed against deionized water for ∼24 h. Unloaded SPIO nanoparticles were then removed via two cycles of centrifugation and redispersion processes.

Drug Release Profile of PTX-Loaded Hybrid Micelles. Hybrid micelles encapsulated with a hydrophobic anticancer drug, PTX, in micellar cores were prepared as follows. Twenty milligrams of PCL$_{70}$-b-PGMA$_{40}$, 4 mg of PCL$_{70}$-b-P(OEGMA$_{0.95}$-co-FA$_{0.05}$)$_{60}$, and 5 mg of PTX were dissolved in 1.0 mL ethanol at 60 °C. Subsequently, 9 mL of deionized water (50 °C) was quickly injected under vigorous stirring. After cooling to room temperature, 1.2 mL aqueous dispersion of CTAB-stabilized SPIO nanoparticles (1.0 g/L) was added. After stirring for 12 h, the dispersion was transferred into dialysis tubing (MW cutoff ∼3.0 kDa) and dialyzed against deionized water for ∼24 h. The remaining micellar solution was then filtered through a 0.45 μm Millipore membrane filter to remove unloaded PTX. To determine the drug loading capacity, all the external dialysis buffer and retained residues after filtration and thorough washing with acetonitrile were combined and freeze-dried. The PTX amount was quantified via UV absorption at 228 nm in acetonitrile against a standard calibration curve. The PTX loading content was determined to be ∼8.5 w/w% relative to polymeric micelles.

The above prepared drug-loaded hybrid micellar dispersion (2.0 mL) was then placed in dialysis tubing (MW cutoff ∼3.0 kDa). The dialysis tubing was immersed into 200 mL of phosphate buffered saline (PBS) buffer (0.02 M, pH 7.4; 37 °C) under continuous gentle stirring. At predetermined time intervals, a 10.0 mL aliquot of external buffer solution was withdrawn and freeze-dried, followed by the addition of 3.0 mL acetonitrile. After each sampling, 10.0 mL of fresh buffer was added to keep constant the total volume of external buffer media. The amount of PTX released was quantified using UV absorbance at 228 nm in acetonitrile against a standard calibration curve.

In Vitro and In Vivo MR Imaging Experiments Using Hybrid Micelles.[47]. For in vitro MRI test of SPIO-loaded hybrid micelles, T_2 was acquired at room temperature using a GE Signa Horizon 1.5 T MR scanner equipped with a human shoulder coil. The T_2-weighted images were acquired with a conventional spin−echo acquisition (TR = 4000 ms) with TE values ranging from 75 to 90 ms. The T_2 relaxivity value, r_2, was calculated via the least-squares curve fitting of $1/T_2$ (s^{-1}) versus Fe concentration plots (mM). For in vivo MR imaging, normal male New Zealand rabbits (∼2.0 kg) were employed for small animal MR imaging tests. The rabbits

were first anesthetized by intravenous injection of ketamine (80 mg/kg) and xylazine (12 mg/kg). Contrast-enhanced images of rabbits were obtained on a GE Signa Horizon 1.5 T MR scanner in a human shoulder coil using the Axial 3D FGRE sequence. The hybrid micellar dispersion was injected via the ear vein into the anesthetized rabbit. Images were acquired at preinjection and different time intervals postinjection of contrast agents. The MR imaging contrast enhancement effects by hybrid micelles were investigated in a group of three rabbits. The relative signal intensities in the region of interest (ROI) at preinjection and postinjection were recorded.

Characterization. All ^{1}H nuclear magnetic resonance (NMR) spectra were recorded on a Bruker AV300 NMR spectrometer (resonance frequency of 300 MHz for ^{1}H) operated in the Fourier transform mode. DMSO-d_6 and CDCl$_3$ were used as the solvent. Molecular weights and molecular weight distributions were determined by GPC equipped with a Waters 1515 pump and a Waters 2414 differential refractive index detector (set at 30 °C). It used a series of three linear Styragel columns (HR3, HR4, and HR6) at an oven temperature of 45 °C. The eluent was DMF at a flow rate of 1.0 mL/min. A series of low polydispersity polystyrene standards were employed for calibration. Fourier transform infrared (FT-IR) spectra were recorded on a Bruker VECTOR-22 IR spectrometer. High-resolution transmission electron microscopy (HRTEM) observations were conducted on a JEOL-2010 electron microscope at an acceleration voltage of 200 kV. All samples for HRTEM observations were prepared by placing 10 μL micellar solution on copper grids coated successively with thin films of Formvar and carbon. Atomic force microscope (AFM) measurements were performed on a Digital Instrument Multimode Nanoscope IIId operating in the tapping mode under ambient conditions. A silicon cantilever (RFESP) with a resonance frequency of ~80 kHz and a spring constant of 3 N/m was used. The set-point amplitude ratio was maintained at 0.7 to minimize sample deformation induced by the tip. All samples were prepared by dip-coating 0.1 g/L aqueous dispersion of hybrid micelles onto freshly cleaved mica surfaces. Dynamic laser light scattering (LLS) measurements were conducted on a commercial spectrometer (ALV/DLS/SLS-5022F) equipped with a multitau digital time correlator (ALV5000) and a cylindrical 22 mW UNIPHASE He—Ne laser (λ_0= 632 nm) as the light source. Scattered light was collected at a fixed angle of 90° for the duration of 5 min. Distribution averages and particle size distributions were computed using cumulants analysis and CONTIN routines. All data were averaged over three measurements. All samples were filtered through 0.45 μm Millipore Acrodisc-12 filters to remove dust.

■ RESULTS AND DISCUSSION

Synthesis of PCL-*b*-P(OEGMA-*co*-FA) and PCL-*b*-PGMA Diblock Copolymers. General synthetic routes employed for the preparation of two types of well-defined amphiphilic block copolymers, PCL-*b*-P(OEGMA-*co*-FA) and PCL-*b*-PGMA, are shown in Scheme 2. In both cases, PCL-based ATRP macroinitiator, PCL$_{70}$-Br, was synthesized at first via the ROP of ε-CL in dry toluene using HBMP as the initiator and Sn(Oct)$_2$ as the catalyst. Previously, we employed trifunctional core molecules bearing hydroxyl and ATRP-initiating bromine moieties for the synthesis of AB$_2$ Y-shaped amphiphilic block copolymers via the combination of ROP and ATRP techniques.[48] GPC analysis of the ROP product revealed an M_n of 9.6 kDa and M_w/M_n of 1.05. The DP of PCL-Br was determined to be 70 by ^{1}H NMR (Figure 1a) from the integral ratio of peak *h* to peak *a*, which are characteristic of PCL repeating units and terminal methyl functionalities, respectively. Thus, the PCL-based macroinitiator

was denoted as PCL$_{70}$-Br and further used for subsequent ATRP processes.

For the synthesis of PCL-*b*-PGMA diblock copolymers, protected GMA monomer, SMA, was polymerized via ATRP at first using PCL$_{70}$-Br macroinitiator, which afforded PCL-*b*-PSMA.[40] The subsequent deprotection reaction of PCL-*b*-PSMA with 1 N HCl in 1,4-dioxane resulted in the formation of amphiphilic PCL-*b*-PGMA diblock copolymer. ^{1}H NMR spectra of PCL-*b*-PSMA precursor and PCL-*b*-PGMA diblock copolymer are shown in Figure 1b,c, respectively, together with the peak assignments. All resonance signals characteristic of PCL and PSMA blocks were clearly visible. The actual DP of the PSMA block was calculated to be 40 based on the integral ratio of resonance peaks characteristic of PCL to that of the PSMA block. Thus, the diblock copolymer was denoted as PCL$_{70}$-*b*-PGMA$_{40}$. GPC analysis of PCL$_{70}$-*b*-PSMA$_{40}$ revealed an $M_{n,GPC}$ of 12.6 kDa and an M_w/M_n of 1.12. The subsequent deprotection of PCL$_{70}$-*b*-PSMA$_{40}$ diblock copolymer afforded amphiphilic diblock copolymer, PCL$_{70}$-*b*-PGMA$_{40}$. The complete removal of protecting groups of PSMA block was evidenced by ^{1}H NMR analysis (Figure 1c). Compared to that of the PCL$_{70}$-*b*-PSMA$_{40}$ precursor, the ^{1}H NMR spectrum of the deprotection product, PCL$_{70}$-*b*-PGMA$_{40}$, clearly revealed the complete disappearance of resonance signal (peak *q*) characteristic of two methyl groups in SMA moieties, confirming the successful synthesis of the target amphiphilic diblock copolymer.[40]

For the synthesis of PCL-*b*-P(OEGMA-*co*-FA) diblock copolymer bearing FA moieties in the hydrophilic block, PCL-*b*-P(OEGMA-*co*-AzPMA) was synthesized at first via the ATRP of OEGMA and AzPMA comonomers using PCL$_{70}$-Br as the macroinitiator, followed by the click reaction with an excess of *alkynyl*-FA. The covalent anchoring of folate moieties in the hydrophilic block allows for the fabrication of diblock copolymer micelles with cancer cell-targeting function. GPC analysis of azide-functionalized PCL-*b*-P(OEGMA-*co*-AzPMA) diblock copolymer revealed an M_n of 24.7 kDa and an M_w/M_n of 1.12. The molar ratio of OEGMA and AzPMA copolymerizing monomers in the hydrophilic block was estimated to be 95:5 from the monomer feed ratio and monomer conversions. In combination with the M_n data determined from GPC, the chemical structure of the final product was determined to be PCL$_{70}$-*b*-P(OEGMA$_{0.95}$-*co*-AzPMA$_{0.05}$)$_{60}$. The calculated DP of P-(OEGMA$_{0.95}$-*co*-AzPMA$_{0.05}$), ~60, also agrees reasonably well with that calculated from ^{1}H NMR spectrum by comparing resonance peak integrals of peak *e* and peak *g*+*g'*, which are characteristic of the PCL block and backbone methyl protons of the P(OEGMA-*co*-AzPMA) block (Figure S1a, Supporting Information).

From the ^{1}H NMR spectrum of PCL-*b*-P(OEGMA-*co*-FA), we can clearly tell that resonance signals characteristic of FA moieties are clearly visible (Figure S1b). Moreover, the FT-IR spectrum (Figure S2) of the PCL-*b*-P(OEGMA-*co*-FA) diblock copolymer revealed the complete disappearance of characteristic azide absorbance peak at ~2100 cm^{-1}, as compared to the PCL-*b*-P(OEGMA-*co*-AzPMA) precursor. This suggested the complete consumption of azide moieties during its click reaction with *alkynyl*-FA and the successful preparation of PCL-*b*-P(OEGMA-*co*-FA) amphiphilic diblock copolymer.[49] Thus, on average, there exist ~3 FA moieties per diblock copolymer chain.

Fabrication of Hybrid Micelles, Drug Loading, and Controlled Release. With the two types of well-defined amphiphilic
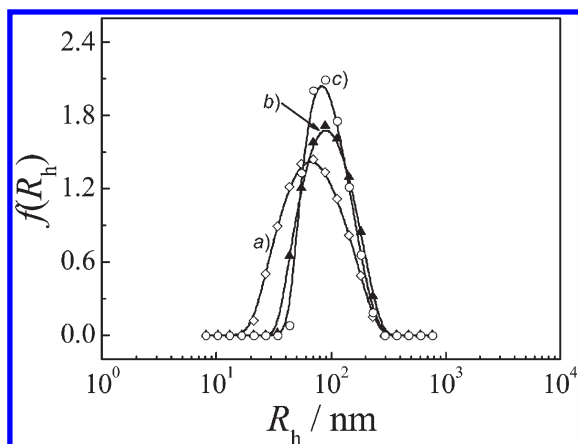
Figure 2. Typical hydrodynamic distributions, $f(R_h)$, recorded for the aqueous dispersion of hybrid micelles comprising hydrophobic PCL cores and mixed PGMA/P(OEGMA-*co*-FA) hydrophilic coronas loaded with 4 nm SPIO nanoparticles fabricated from PCL-*b*-PGMA and PCL-*b*-P(OEGMA-*co*-FA) diblock copolymers (5/1, w/w) at varying SPIO loading contents ($W_{SPIO}/W_{micelles}$, w/w%): (a) 0, (b) 5%, and (c) 10%. The concentration of mixed micelles was 0.2 g/L.
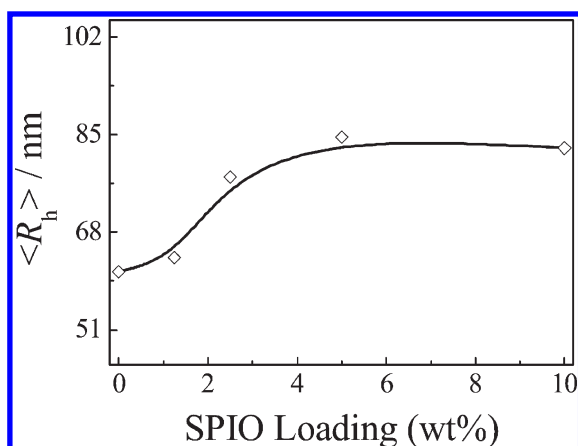
Figure 3. The variation of intensity-average hydrodynamic radius, $\langle R_h \rangle$, as a function of SPIO loading content ($W_{SPIO}/W_{mixed\ micelles}$, w/w%) for hybrid micelles comprising hydrophobic PCL cores and mixed PGMA/P(OEGMA-*co*-FA) hydrophilic coronas loaded with SPIO nanoparticles (4 nm) from PCL-*b*-PGMA and PCL-*b*-P(OEGMA-*co*-FA) diblock copolymers (5/1, w/w). The concentration of mixed micelles was fixed at 0.2 g/L.

diblock copolymers, PCL$_{70}$-*b*-PGMA$_{40}$ and PCL$_{70}$-*b*-P-(OEGMA$_{0.95}$-*co*-FA$_{0.05}$)$_{60}$, in hand, we then fabricated mixed micelles possessing hydrophobic PCL cores and hydrophilic mixed coronas of PGMA and FA-labeled P(OEGMA-*co*-AzPMA) (Scheme 1). It is well-established that hydrophobic anticancer drugs such as PTX can be physically encapsulated within the micellar cores.[31−33] The micellar nanocarriers can exert the controlled-release feature to loaded drug molecules. As previously reported by Wan et al.,[40] 1,2-diol moieties in PGMA can exhibit high affinity with Fe atoms at the surface of SPIO nanoparticles, and PGMA can act as excellent stabilizing ligands for SPIO nanoparticles. Thus, we propose that PGMA sequences in the hydrophilic coronas of mixed micelles are fabricated from PCL$_{70}$-*b*-PGMA$_{40}$ and PCL$_{70}$-*b*- P(OEGMA$_{0.95}$-*co*-FA$_{0.05}$)$_{60}$ diblock copolymers. On the other hand, the FA-labeled
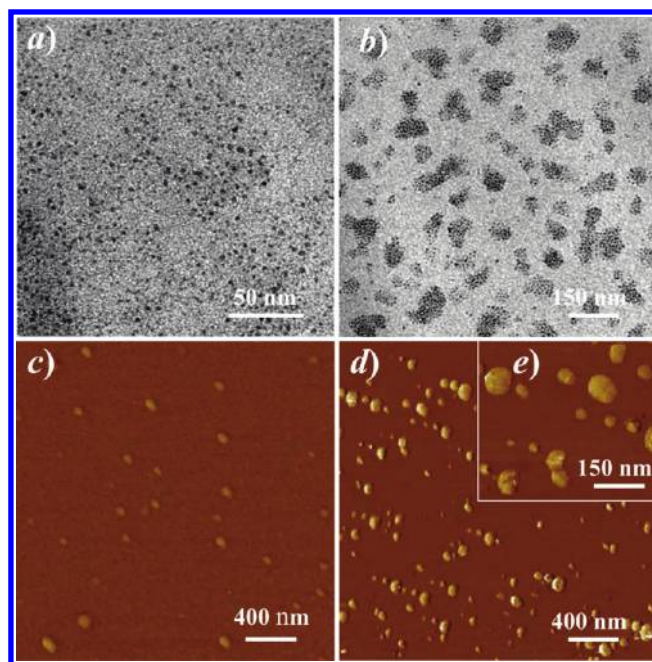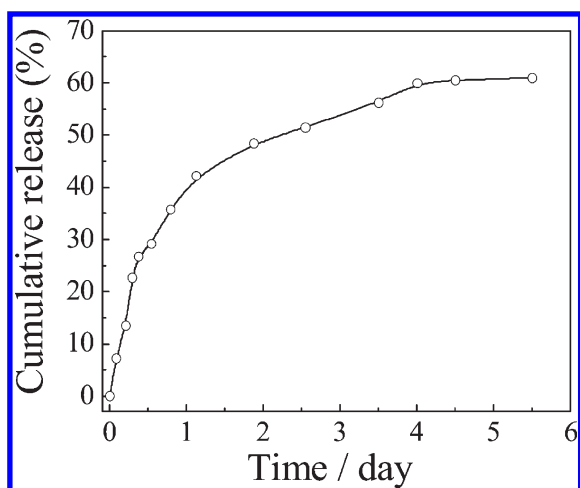

Figure 4. Typical HRTEM images obtained for (a) CTAB-stabilized 4 nm SPIO nanoparticles and (b) hybrid micelles comprising of hydrophobic PCL cores and mixed PGMA/P(OEGMA-*co*-FA) hydrophilic coronas loaded with 5.0 w/w% SPIO nanoparticles (4 nm) fabricated from PCL-*b*-PGMA and PCL-*b*-P(OEGMA-*co*-FA) diblock copolymers (5/1, w/w). AFM height images obtained for (c) mixed micelles before loaded with SPIO nanoparticles and (d,e) hybrid micelles.

P(OEGMA-*co*-FA) block in the mixed micellar coronas can exhibit two advantages for the multifunctional nanocarriers: (1) the presence of FA moieties can endow mixed micelles with the capability of specifically targeting FA overexpressing cancer cells; and (2) the P(OEGMA-*co*-FA) sequence, with its DP (60) larger than that of PGMA chain sequence (40), can act as hydrophilic steric stabilizer for hybrid micelles with the coronas surface loaded with SPIO nanoparticles.

Dynamic LLS measurements of mixed micelles fabricated from PCL$_{70}$-*b*-PGMA$_{40}$ and PCL$_{70}$-*b*-P(OEGMA$_{0.95}$-*co*-FA$_{0.05}$)$_{60}$ at a weight ratio of 5/1 revealed an intensity-average hydrodynamic radius, $\langle R_h \rangle$, of ∼61 nm before corona-embedding with SPIO nanoparticles (Figures 2 and 3). For mixed micelles, R_h is in the range of 15−300 nm, exhibiting a size polydispersity (μ_2/Γ^2) of ∼0.12. Upon loading with 5.0 w/w% of 4 nm SPIO nanoparticles, the hydrodynamic radius distribution clearly shifted to larger values (Figure 2), exhibiting a $\langle R_h \rangle$ of 84 nm and a μ_2/Γ^2 of 0.16. This clearly confirmed the loading of SPIO nanoparticles into micellar coronas due to strong affinity between hydrophilic PGMA sequences and iron oxide nanoparticles (Scheme 1).

Furthermore, Figure 2 shows that when the SPIO nanoparticle loading content was increased to 10.0 w/w%, the hydrodynamic radius distribution of hybrid micelles does not exhibit appreciable changes as compared to that at 5.0 w/w%. This suggests that 5.0 w/w% nanoparticle loading is close to the saturating loading value; at this nanoparticle loading amount, almost all binding sites on PGMA sequences in the micellar coronas were occupied. Thus, in subsequent sections, the SPIO loading content was fixed at 5.0 w/w% relative to the polymeric micelles. It is worth noting
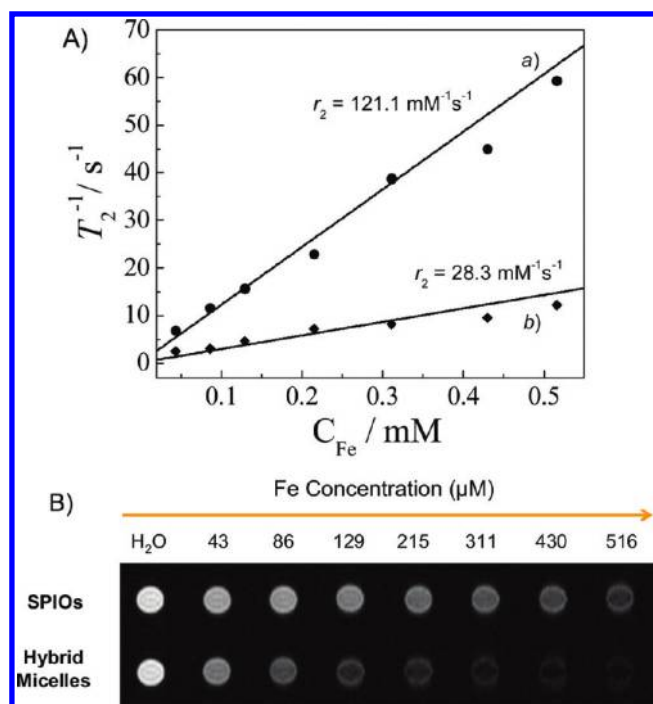
Figure 5. Cumulative release (37 °C and pH 7.4) of PTX (loading content ~8.5 w/w%) from drug-loaded hybrid micelles comprising hydrophobic PCL cores and mixed PGMA/P(OEGMA-co-FA) hydrophilic coronas embedded with 5 w/w% SPIO nanoparticles (4 nm) fabricated from PCL-b-PGMA and PCL-b-P(OEGMA-co-FA) diblock copolymers (5/1, w/w).

that hydrophilic SPIO nanoparticles were loaded after the formation of mixed micelles from PCL_{70}-b-$PGMA_{40}$ and PCL_{70}-b-$P(OEGMA_{0.95}$-co-$FA_{0.05})_{60}$. Thus, these nanoparticles will not enter into the hydrophobic PCL cores. Because POEGMA exhibits negligible binding affinity with iron oxide nanoparticles, the embedding of SPIO nanoparticles into the micellar coronas should be solely ascribed to the presence of hydrophilic PGMA sequences.[40] Figure 4 shows typical HRTEM images of CTAB-stabilized SPIO nanoparticles and nanoparticle-loaded hybrid micelles. We can clearly tell that CTAB-stabilized SPIO nanoparticles are well-dispersed, exhibiting an average diameter of ~4 nm (Figure 4a); whereas for hybrid micelles, we can observe the presence of robust SPIO nanoparticle clusters. We can only see nanoparticle clusters because polymeric micelles exhibit considerably lower attenuation effect to electron beams compared to that by iron oxide nanoparticles. However, the clustering of nanoparticles as observed by TEM clearly confirmed that SPIO nanoparticles were successfully loaded into the micellar coronas.

Figure 4c,d also shows AFM images of mixed micelles before and after loading with SPIO nanoparticles. Mixed micelles of PCL_{70}-b-$PGMA_{40}$ and PCL_{70}-b- $P(OEGMA_{0.95}$-co-$FA_{0.05})_{60}$ before SPIO nanoparticle loading appear as almost spherical nanospheres (Figure 4c). After nanoparticle loading, hybrid micelles exhibit enhanced contrast in the AFM height image. Moreover, we can even discern the presence of SPIO nanoparticles from Figure 4e (inset). It seems that the SPIO nanoparticles are relatively densely packed within micellar coronas. The loading of SPIO nanoparticles into micellar coronas can also be evidenced from thermogravimetric analysis (TGA) (Figure S3), revealing weight retentions of ~62% and ~6.1% for CTAB-stabilized SPIO nanoparticles and SPIO nanoparticle-loaded hybrid micelles, respectively. Overall, the above dynamic LLS, TEM, and AFM results verified that SPIO nanoparticles were successfully embedded into micellar coronas thanks to the strong affinity between PGMA and iron oxide nanoparticles.

A model hydrophobic anticancer drug, PTX, was further encapsulated into the micellar cores of SPIO nanoparticle-loaded


Figure 6. (A) T_2 relaxation rates $(1/T_2)$ as a function of iron concentration recorded for the aqueous dispersion (25 °C) of (a) CTAB-stabilized SPIO nanoparticles and (b) hybrid micelles comprising hydrophobic PCL cores and mixed PGMA/P(OEGMA-co-FA) hydrophilic coronas embedded with ~5 w/w% SPIO nanoparticles (4 nm) fabricated from PCL-b-PGMA and PCL-b-P(OEGMA-co-FA) diblock copolymers (5/1, w/w). (B) T_2-weighted MRI images obtained for CTAB-stabilized SPIO nanoparticles and hybrid micelles, respectively.

hybrid micelles. For the drug loading, hybrid micelles were prepared via the nanoprecipitation approach in the presence of PTX, followed by surface embedding with SPIO nanoparticles. The drug loading content was determined to be 8.5 w/w% relative to polymeric micelles, corresponding to a drug encapsulation efficiency of ~41%. The drug release profile from hybrid micelles was further examined, and the results are shown in Figure 5. We can tell that sustained release of PTX from hybrid micelles was achieved. Cumulatively, ~61% of loaded PTX was released over a period of ~130 h. A closer examination of Figure 5 revealed that 40% encapsulated PTX was released over the first 24 h. On the basis of the TEM and AFM results shown in Figure 4, we speculate that SPIO nanoparticle-loaded hybrid micelles might to some extent act as shell cross-linked micelles because SPIO nanoparticles in the micellar coronas can actually physically cross-link PGMA chains;[50,51] this might exert some advantageous effects for the secondary modulation of drug release profile in addition to the diffusing barrier of hydrophobic micellar cores. Moreover, the hybrid micelles contain cancer cell-targeting FA moieties, thus, drug-loaded hybrid micelles are capable of targeting specific type of cancer cells and tissues. Further experiments toward the evaluation of cytotoxicity of hybrid micellar nanocarriers before and after loading with PTX and the intracellular delivery of anticancer drugs are currently underway.

In Vitro and In Vivo MR Imaging Tests of SPIO-Loaded Hybrid Micelles. SPIO nanoparticles have been clinically used as a T_2-type MR imaging contrast agents, which are commercially
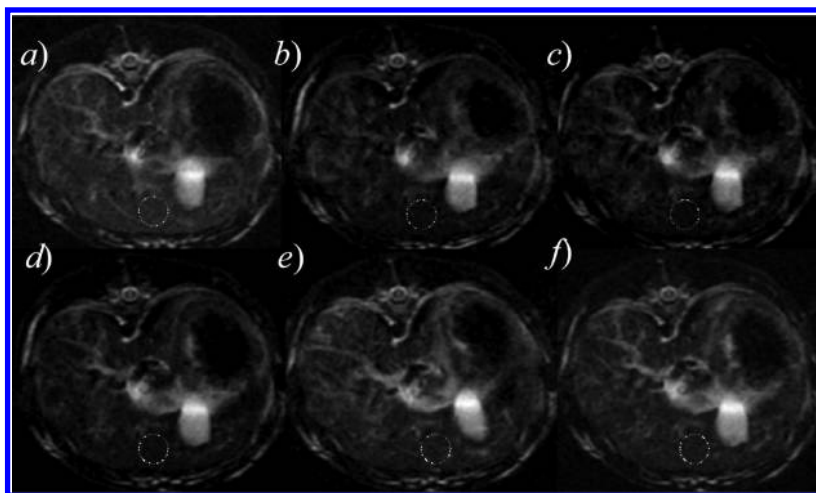
Figure 7. T_2-weighted MR images of the rabbit liver recorded (a) before and (b–f) after injection of hybrid micelles comprising of hydrophobic PCL cores and mixed PGMA/P(OEGMA-*co*-FA) hydrophilic coronas embedded with 5 w/w% SPIO nanoparticles (4 nm) fabricated from PCL-*b*-PGMA and PCL-*b*-P(OEGMA-*co*-FA) diblock copolymers (5/1, w/w) at varying time periods: (b) 5 min, (c) 9 min, (d) 18 min, (e) 27 min, and (f) 24 h.
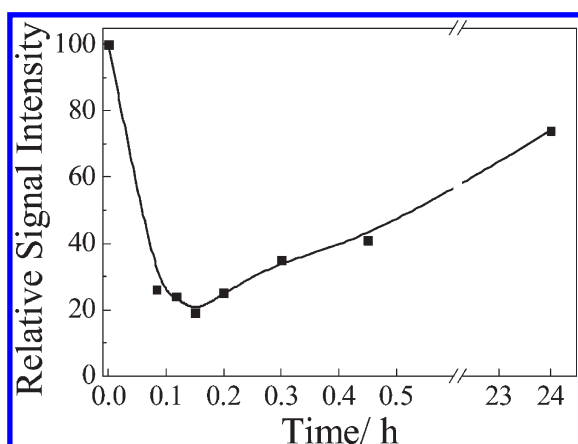
Figure 8. Signal-to-noise ratio (SNR) at the marked position as a function of time in rabbit liver after intravenous injection of hybrid micelles comprising hydrophobic PCL cores and mixed PGMA/P-(OEGMA-*co*-FA) hydrophilic coronas loaded with ~5 w/w% SPIO nanoparticles (4 nm) fabricated from PCL-*b*-PGMA and PCL-*b*-P-(OEGMA-*co*-FA) diblock copolymers (5/1, w/w).

available as several brand names.[52] Several previous reports established that when SPIO nanoparticles are present as clusters within polymeric micellar cores, the T_2 relaxivity (r_2) can be considerably enhanced due to collective effects of nanoparticle assemblies.[25−30] In the current study, hydrophilic SPIO nanoparticles were embedded into the well-solvated coronas of amphiphilic diblock copolymer micelles (Scheme 1). Thus, it is quite intriguing to check whether this new type of design can still allow for the fabrication of a hybrid micelle-based MR imaging contrast enhancer. If that is the case, hybrid micelles with hydrophobic cores and hydrophilic coronas respectively loaded with anticancer drugs and SPIO nanoparticles should act as a new type of nanoplatform for the fabrication of image-guided drug delivery and integrated theranostic nanocarriers.

Typical T_2 weighted spin−echo MR images recorded for hybrid micelles of PCL$_{70}$-*b*-PGMA$_{40}$ and PCL$_{70}$-*b*-P(OEGMA$_{0.95}$-*co*-FA$_{0.05}$)$_{60}$ (5/1, w/w) at a SPIO nanoparticle loading content of

5.0 w/w% are shown in Figure 6B. The performance of CTAB-stabilized 4 nm SPIO nanoparticles was employed as a reference. Upon gradually increasing the concentration of single SPIO nanoparticles, we can observe a gradual increase of negative contrast enhancement of MR signals, as revealed by the darkening of detection spots. Moreover, the corresponding SPIO nanoparticle-embedded hybrid micelles exhibit substantially faster MR signal contrast enhancement in the same Fe concentration range. This confirms that even when hydrophilic SPIO nanoparticles are embedded in the well-solvated coronas of mixed micelles (Scheme 1), their clustering (as shown in Figure 4) can lead to enhanced T_2-type MR imaging contrast.

We further conducted quantitative analysis to investigate the enhancement of MR imaging contrast (Figure 6A). Data analysis based on Matlab software indicated a linear relationship between water proton transverse relaxation rate ($1/T_2$) and Fe concentrations. CTAB-stabilized 4 nm SPIO nanoparticles possess a T_2 relaxivity (r_2) of 28.3 s^{-1} mM^{-1} Fe, which is in reasonable agreement with that reported for single SPIO nanoparticles in the literature.[52] On the other hand, linear regression analysis of a $1/T_2$ versus [Fe] plot for hybrid micelles revealed considerably enhanced contrast efficiency, as evidenced by the much larger slope of the plot compared to that for CTAB-stabilized 4 nm SPIO nanoparticles. For hybrid micelles, the T_2 relaxivity (r_2) was calculated to be 121.1 s^{-1} mM^{-1} Fe. Thus, ~4.3-fold enhancement T_2 relaxivity was achieved in comparison with that of single SPIO nanoparticles. These results verified well that SPIO nanoparticle surface-loaded hybrid micelles can serve as excellent T_2-type contrast agents integrated with targeted drug delivery and controlled release characteristics.

Finally, we conducted preliminary in vivo MR imaging tests using SPIO nanoparticle-loaded hybrid micelles, and the results are shown in Figures 7 and 8. Figure 7 shows T_2-weighted MR images of the rabbit liver organ, which were acquired before and at different time points after the intravenous injection of hybrid micelles. Using the MR image before injection as a control, we can clearly observe the quick darkening of the liver organ (see the circle for ROI) quickly after the injection. At extended time periods, the signal intensities partially recovered. From Figure 8, we can tell that the relative signal intensities reached its minimum

($\sim$19%) at $\sim$9 min postinjection. After that, the signal intensity gradually increased with time. At $\sim$24 h postinjection, the relative signal intensity restored to $\sim$74% of the original value before intravenous injection of hybrid micelles. Thus, the T_2-type contrast enhancement of SPIO nanoparticle-embedded hybrid micelles is quite comparable to those of clinically approved liver contrast agents (e.g., Feridex and Resovist), which also exert considerable signal changes quickly after SPIO nanoparticle injection.[53] From Figure 8, we can also tell that the time window suitable for MR imaging is within 30 min after the injection of hybrid micelles, as the relative signal intensities in this time frame are typically less than $\sim$40% of the original value.

CONCLUSION

Organic/inorganic hybrid micelles of amphiphilic block copolymers physically encapsulated with hydrophobic drugs within micellar cores and stably embedded with SPIO nanoparticles within hydrophilic coronas were fabricated, which possess integrated functions of chemotherapeutic drug delivery and MR imaging contrast enhancement. Drug-loaded and SPIO nanoparticle-embedded hybrid micelles exert controlled and sustained release of PTX from hydrophobic micellar cores, exhibiting a cumulative release of $\sim$61% encapsulated drugs (loading content, 8.5 w/w%) over $\sim$130 h. Compared to that of CTAB-stabilized single SPIO nanoparticles ($r_2 = 28.3 \ \text{s}^{-1} \ \text{mM}^{-1}$ Fe), the clustering of SPIO nanoparticles within micellar coronas led to $\sim$4.3 times enhancement in T_2 relaxivity ($r_2 = 121.1 \ \text{s}^{-1} \ \text{mM}^{-1}$ Fe), suggesting that hybrid micelles with corona-embedded SPIO nanoparticle clusters can serve as a T_2-weighted MR imaging contrast enhancer with improved performance. In addition, preliminary experiments show that these hybrid micelles can be also applied as an in vivo small animal MR imaging contrast agent. Overall, we established that amphiphilic block copolymer micelle surfaces embedded with SPIO nanoparticle clusters at the hydrophilic corona can act as a new generation of multifunctional agents integrated with targeted drug delivery, controlled release, and disease diagnostic functions.

ASSOCIATED CONTENT

Ⓢ Supporting Information. ^{1}H NMR spectra recorded for PCL$_{70}$-b-P(OEGMA$_{0.95}$-co-AzPMA$_{0.05}$)$_{60}$ in CDCl$_3$ and PCL$_{70}$-b-P(OEGMA$_{0.95}$-co-FA$_{0.05}$)$_{60}$ in DMSO-d$_6$. FT-IR spectra recorded for PCL$_{70}$-b-P(OEGMA$_{0.95}$-co-AzPMA$_{0.05}$)$_{60}$ and PCL$_{70}$-b-P(OEGMA$_{0.95}$-co-FA$_{0.05}$)$_{60}$ diblock copolymers. TGA curves recorded for CTAB-stabilized 4 nm SPIO nanoparticles and hybrid micelles comprising hydrophobic PCL cores and mixed PGMA/P(OEGMA-co-FA) hydrophilic coronas embedded with 4 nm SPIO nanoparticles fabricated from PCL-b-PGMA and PCL-b-P(OEGMA-co-FA) diblock copolymers (5/1, w/w). This material is available free of charge via the Internet at http://pubs.acs.org.

AUTHOR INFORMATION

Corresponding Author

*To whom correspondence should be addressed. E-mail: sliu@ustc.edu.cn (S.L.); liangminqyf@sohu.com (Y.Q.).

ACKNOWLEDGMENT

REFERENCES

(1) Janib, S. M.; Moses, A. S.; MacKay, J. A. *Adv. Drug Delivery Rev.* **2010**, *62*, 1052–1063.

(2) Kim, J.; Piao, Y.; Hyeon, T. *Chem. Soc. Rev.* **2009**, *38*, 372–390.

(3) Davis, M. E.; Chen, Z.; Shin, D. M. *Nat. Rev. Drug Discovery* **2008**, *7*, 771–782.

(4) Ferrari, M. *Nat. Rev. Cancer* **2005**, *5*, 161–171.

(5) Duncan, R. *Nat. Rev. Drug Discovery* **2003**, *2*, 347–360.

(6) Ansari, A. A.; Alhoshan, M.; Alsalhi, M. S.; Aldwayyan, A. S. *Sensors* **2010**, *10*, 6535–6581.

(7) Villaraza, A. J. L.; Bumb, A.; Brechbiel, M. W. *Chem. Rev.* **2010**, *110*, 2921–2959.

(8) Aime, S.; Terreno, E.; Castelli, D. D.; Viale, A. *Chem. Rev.* **2010**, *110*, 3019–3042.

(9) von Rechenberg, B.; Neuberger, T.; Schopf, B.; Hofmann, H.; Hofmann, M. *J. Magn. Magn. Mater.* **2005**, *293*, 483–496.

(10) Richardson, J.; Bowtell, R.; Mader, K.; Melia, C. *Adv. Drug Delivery Rev.* **2005**, *57*, 1191–1209.

(11) Ma, Z. Y.; Liu, H. Z. *China Particuol.* **2007**, *5*, 1–10.

(12) Duan, H. W.; Kuang, M.; Wang, X. X.; Wang, Y. A.; Mao, H.; Nie, S. M. *J. Phys. Chem. C* **2008**, *112*, 8127–8131.

(13) Bulte, J. W. M.; Kraitchman, D. L. *NMR Biomed.* **2004**, *17*, 484–499.

(14) Gomm, J. J.; Browne, P. J.; Coope, R. C.; Liu, Q. Y.; Buluwela, L.; Coombes, R. C. *Anal. Biochem.* **1995**, *226*, 91–99.

(15) Lee, J. H.; Huh, Y. M.; Jun, Y.; Seo, J.; Jang, J.; Song, H. T.; Kim, S.; Cho, E. J.; Yoon, H. G.; Suh, J. S.; Cheon, J. *Nat. Med.* **2007**, *13*, 95–99.

(16) Lewin, M.; Carlesso, N.; Tung, C. H.; Tang, X. W.; Cory, D.; Scadden, D. T.; Weissleder, R. *Nat. Biotechnol.* **2000**, *18*, 410–414.

(17) Medarova, Z.; Pham, W.; Farrar, C.; Petkova, V.; Moore, A. *Nat. Med.* **2007**, *13*, 372–377.

(18) Smith, J. E.; Medley, C. D.; Tang, Z. W.; Shangguan, D.; Lofton, C.; Tan, W. H. *Anal. Chem.* **2007**, *79*, 3075–3082.

(19) Nie, Z. H.; Petukhova, A.; Kumacheva, E. *Nat. Nanotechnol.* **2010**, *5*, 15–25.

(20) Kumar, P. *Nanoscale Res. Lett.* **2010**, *5*, 1367–1376.

(21) Grzelczak, M.; Vermant, J.; Furst, E. M.; Liz-Marzan, L. M. *ACS Nano* **2010**, *4*, 3591–3605.

(22) Qian, X. M.; Li, J.; Nie, S. M. *J. Am. Chem. Soc.* **2009**, *131*, 7540–7541.

(23) Kneipp, J.; Kneipp, H.; Kneipp, K. *Chem. Soc. Rev.* **2008**, *37*, 1052–1060.

(24) Yin, J.; Wu, T.; Song, J.; Zhang, Q.; Liu, S.; Xu, R.; Duan, H. *Chem. Mater.* **2011**, DOI: 10.1021/cm201791r.

(25) Lattuada, M.; Hatton, T. A. *J. Am. Chem. Soc.* **2007**, *129*, 12878–12889.

(26) Sondjaja, R.; Hatton, T. A.; Tam, M. K. C. *J. Magn. Magn. Mater.* **2009**, *321*, 2393–2397.

(27) Ai, H.; Flask, C.; Weinberg, B.; Shuai, X. T.; Pagel, M. D.; Farrell, D.; Duerk, J.; Gao, J. M. *Adv. Mater.* **2005**, *17*, 1949–1952.

(28) Kim, B. S.; Qiu, J. M.; Wang, J. P.; Taton, T. A. *Nano Lett.* **2005**, *5*, 1987–1991.

(29) Berret, J. F.; Schonbeck, N.; Gazeau, F.; El Kharrat, D.; Sandre, O.; Vacher, A.; Airiau, M. *J. Am. Chem. Soc.* **2006**, *128*, 1755–1761.

(30) Euliss, L. E.; Grancharov, S. G.; O'Brien, S.; Deming, T. J.; Stucky, G. D.; Murray, C. B.; Held, G. A. *Nano Lett.* **2003**, *3*, 1489–1493.

(31) Adams, M. L.; Lavasanifar, A.; Kwon, G. S. *J. Pharm. Sci.* **2003**, *92*, 1343–1355.

(32) Attia, A. B. E.; Ong, Z. Y.; Hedrick, J. L.; Lee, P. P.; Ee, P. L. R.; Hammond, P. T.; Yang, Y. Y. *Curr. Opin. Colloid Interface Sci.* **2011**, *16*, 182–194.

(33) Torchilin, V. P. *Adv. Drug Delivery Rev.* **2002**, *54*, 235–252.

(34) Ge, Z. S.; Xu, J.; Hu, J. M.; Zhang, Y. F.; Liu, S. Y. *Soft Matter* **2009**, *5*, 3932–3939.

(35) Xu, J.; Liu, S. Y. *Soft Matter* **2008**, *4*, 1745–1749.

(36) Nasongkla, N.; Bey, E.; Ren, J.; Ai, H.; Khemtong, C.; Guthi, J. S.; Chin, S. F.; Sherry, A. D.; Boothman, D. A.; Gao, J. M. *Nano Lett.* **2006**, *6*, 2427–2430.

(37) Guthi, J. S.; Yang, S. G.; Huang, G.; Li, S.; Khemtong, C.; Kessinger, C. W.; Peyton, M.; Minna, J. D.; Brown, K. C.; Gao, J. M. *Mol. Pharmaceutics* **2009**, *7*, 32–40.

(38) Yang, X. Q.; Grailer, J. J.; Rowland, I. J.; Javadi, A.; Hurley, S. A.; Steeber, D. A.; Gong, S. Q. *Biomaterials* **2010**, *31*, 9065–9073.

(39) Yang, X. Q.; Grailer, J. J.; Rowland, I. J.; Javadi, A.; Hurley, S. A.; Matson, V. Z.; Steeber, D. A.; Gong, S. Q. *ACS Nano* **2010**, *4*, 6805–6817.

(40) Wan, S. R.; Zheng, Y.; Liu, Y. Q.; Yan, H. S.; Liu, K. L. *J. Mater. Chem.* **2005**, *15*, 3424–3430.

(41) Sumerlin, B. S.; Tsarevsky, N. V.; Louche, G.; Lee, R. Y.; Matyjaszewski, K. *Macromolecules* **2005**, *38*, 7540–7545.

(42) De, P.; Gondi, S. R.; Sumerlin, B. S. *Biomacromolecules* **2008**, *9*, 1064–1070.

(43) Mori, H.; Hirao, A.; Nakahama, S.; Senshu, K. *Macromolecules* **1994**, *27*, 4093–4100.

(44) Mori, H.; Hirao, A.; Nakahama, S. *Macromolecules* **1994**, *27*, 35–39.

(45) Frey, H.; Wolf, F. F.; Friedemann, N. *Macromolecules* **2009**, *42*, 5622–5628.

(46) Si, S.; Kotal, A.; Mandal, T. K.; Giri, S.; Nakamura, H.; Kohara, T. *Chem. Mater.* **2004**, *16*, 3489–3496.

(47) Li, X. J.; Qian, Y. F.; Liu, T.; Hu, X. L.; Zhang, G. Y.; You, Y. Z.; Liu, S. Y. *Biomaterials* **2011**, *32*, 6595–6605.

(48) Liu, H.; Xu, J.; Jiang, J. L.; Yin, J.; Narain, R.; Cai, Y. L.; Liu, S. Y. *J. Polym. Sci., Part A: Polym. Chem.* **2007**, *45*, 1446–1462.

(49) Xu, J.; Ye, J.; Liu, S. Y. *Macromolecules* **2007**, *40*, 9103–9110.

(50) Liu, S. Y.; Weaver, J. V. M.; Save, M.; Armes, S. P. *Langmuir* **2002**, *18*, 8350–8357.

(51) Liu, S. Y.; Weaver, J. V. M.; Tang, Y. Q.; Billingham, N. C.; Armes, S. P.; Tribe, K. *Macromolecules* **2002**, *35*, 6121–6131.

(52) Gupta, A. K.; Gupta, M. *Biomaterials* **2005**, *26*, 3995–4021.

(53) Reimer, P.; Balzer, T. *Eur. Radiol.* **2003**, *13*, 1266–1276.